

Combined AFM/Raman microspectroscopy for characterization of living cells in near physiological conditions

A.H. Zhou, G.D. McEwen, and Y.Z. Wu

Department of Biological Engineering, Utah State University, Logan, Utah 84322-4105, U.S.A

Raman microspectroscopy (RM) is a noninvasive, label-free, molecular spectroscopy method used to record the vibrational spectroscopic fingerprints based on molecular bonds and has been recently applied to characterize living cells. Atomic force microscopy (AFM) is a high-resolution form of scanning probe microscopy that can provide information including surface topography, cell adhesion, and cellular elasticity of single cell. By exploiting the advantages of these two microscopies, we have applied a combined AFM/RM technique to investigate both biomechanical and biochemical properties of living cells in near physiological conditions. The model cells involved were bacterial cells (e.g. *Pseudomonas putida*) and mammalian cells (e.g. human lung cancer cells and breast cancer cells) in physiological conditions. The overall objective of this chapter is to provide new insightful information on molecular structural, cell cytoarchitectural, and biomechanical properties from bacterial cells to human cancer cells at the single cell level, and to discuss applications of combined AFM/RM in single cell studies.

Keywords Raman microspectroscopy; atomic force microscopy; biological cells; bacteria; breast cancer; lung cancer

1. Introduction

It is known that the mechanical forces of cells play a fundamental role in the regulation of cell structures and functions. However, characterization of cell mechanics at the single cell level still remains challenging due to the lack of applicable force-sensitive technologies that can achieve nanoscale resolutions. Conventional microscopy like optical microscopes allow live cell imaging, but their resolution is limited (diffraction limitation) and sample prestaining is often required. Electron microscopes (including scanning (SEM) and transmission (TEM) types) can reach nanometer scale resolutions, but samples must undergo a series of pretreatments; such as fixation, dehydration, and subsequent imaging must be performed in a vacuum, which thus fails to provide native structural information of the cells in (near) physiological environment. Moreover, these microscopy techniques cannot reveal any information about cellular mechanical properties. Atomic force microscopy (AFM) was developed from scanning tunneling microscopy (STM) in the 1980's [1] and works differently compared with optical microscopy and electron microscopy. It obtains sample topographical structures by detecting dynamic variation of interaction force between the AFM tip and the sample surface when AFM tip scanning across a sample surface [2]. AFM possesses unique advantages over other types of microscopies [2, 3], for example, AFM measurements can be performed in near-physiological conditions [4, 5], sample preparation is simplified, and the ability to simultaneously achieve the visualizations of nanostructures and the detection of nanomechanics of cell samples [2, 3]. Therefore, the development of AFM pioneered new applications in the field of microscopy, and it has provided new opportunities and insights into nano-biology [6]. In the past decades, AFM, as a valuable force (nN/pN)-sensitive technique, had been widely applied in cell biological studies [2, 3, 7, 8].

Raman microspectroscopy (RM) is a nondestructive vibrational classification method that can be utilized to identify characteristic spectroscopic fingerprints of bacteria [9, 10] and living cells [11] based on chemical composition and molecular structures. In the course of recent decades, RM has gained more popularity in bacterial [9, 12-16] and mammalian cell [17-19] characterization due to advances in instrumentation design [20, 21], meaningful biological approaches [22, 23], and data mining methods for biochemical information extraction [15, 24]. As advances have progressed, so has the scope and application of RM within the fields of life science and clinical research. RM has been utilized to identify and differentiate specific bacteria; such as, Gram-positive *Bacillus anthracis*, *B. thuringensis*, and *B. atrophaeus* spores, and *B. cereus* vegetative cells by using Raman imaging and data analysis routines [25] and rapid "finger-printing" combined with principal component analysis (PCA) has been used to discriminate simulated biological threats [26]. Furthermore, RM has been used to study subcellular drug distribution of paclitaxel within breast cancer cells [11] and to diagnose breast cancer based on differences within normal, malignant, and benign tissues [27, 28]. Other examples of Raman work with cancer are cervical cancer pathology [24, 29] and pre-cancer discrimination [30], specific biomarkers for normal and adenocarcinomatous colonic tissue [31], and biological effects of diesel exhaust particels (DEP) on bronchial epithelial cells [32] and human lung adenocarcinoma cell interaction with *Jasada Bhasma* [33].

The objective of the present work is to discuss the usefulness of combining Raman microspectroscopy and AFM technologies in the detection of biochemical compositions and nanomechanics of bacterial cells (*Pseudomonas putida* KT2440) and mammalian cancer cells (metastatic human breast carcinoma cells MDA-MB-435, non-metastatic MDA-MB-435/BRMS1, and human lung adenocarcinoma epithelial A549 cells).

2. AFM/Raman microspectroscopy for bacterial studies

2.1 Biological Background and Rationale

The Gram-negative bacterial cell wall is compiled of an outer membrane, the periplasmic space, and an inner membrane. The outer membrane is made up of lipopolysaccharides (LPS) and is the first line of defense for Gram-negative bacteria, serves as a protection barrier [34], and maintains the cell rigidity and shape [35]. The outer membrane structures are hydrophobic and directly exposed to the outside environment [35]. Therefore, the studies of nanostructures and adhesion behaviours of the outer cell wall are of interest for further understanding of the adhesion related biological processes. Here, the Gram-negative bacterium derivative *Pseudomonas putida* KT2440 was selected as a model bacterial strain for AFM/Raman analysis. *P. putida* strain mt-2 (the toluene-degrading isolate) and was considered as the first biosafety strain by the Recombinant DNA Advisory Committee [36-38] and thus was used in our studies. In this subsection, AFM techniques and Raman microspectroscopy will be utilized to characterize extracellular polymeric substances (EPS) and nanostructural features specific to the KT2440 cell wall outer membrane.

2.2 AFM and Raman Imaging

For AFM analysis, KT2440 were grown in Luria Broth (LB) culture media composed of yeast extract, peptone from casein and sodium chloride (mass ratio, 1:2:1) at room temperature. Bacteria from the exponential growth phase were centrifuged for 2 min at 2000 rpm (Eppendorf Minispan), then 5 μ l of bacteria were dropped onto a clean cover glass substrate and allowed to dry in air (less than 1 minute) (*P. Putida* KT2440 did not undergo any additional treatment). Next, the contact mode AFM (Picoplus, Agilent Technologies, USA) was used to measure bacterial cells at room temperature in air. The spring constant of the cantilevers (Veeco Inc. USA) used in the experiments was 0.12 N/m, and the curvature radius of Si_3N_4 tip is approximately 10 nm. The values of adhesion force (the interaction force between bare AFM tip and cell surface) were extracted from curves of deflection (nm) vs. distance (nm) via the software Scanning Probe Image Processor (SPIP) (Image Metrology, Denmark). All statistical data were reported as mean \pm SE (standard error of the mean), and the histograms were created using OriginPro 7.5 (OriginLab Corp., USA). For the analysis using Raman spectroscopy, *P.putida* KT2440 were grown on LB agar composed of yeast extract, peptone from casein, sodium chloride, and agar (mass ratio, 1:2:1:3) at room temperature in air. The agar plate containing KT2440 was inoculated and after 24 hours was transferred onto the stage of Renishaw inVia Raman microscope (with 785 nm laser) for observation and spectral measurements. Raman spectra were collected in a static mode of three accumulations with 10 second laser exposure and were an average of twelve individual Raman spectra. All wavenumber ranges for each spectra were truncated to 600 – 1800 cm^{-1} and pre-processed by Savitsky-Golay smoothing and fluorescence correction [39]. The Raman spectral image of KT2440 was imaged at a static wavenumber of 1006 cm^{-1} over a set range of ~816 - 1186 cm^{-1} , with 45 second exposure time at 100% laser power and was smoothed via bilinear interpolation. All Raman results for KT2440 are discussed in section 3.3 below.

2.3 Results and Quantification

One of characteristic for Gram-negative bacterial cells is their flagellum structures, which play an important role in the functionalization of biological processes (e.g. motility, swimming, adhesion, etc.). AFM was thus used to detect the difference in adhesion properties between the flagella and the bacterial cell wall (**Fig. 1**). First, the measurements quantified the diameter of the bacterial flagella, which was measured at 69.6 \pm 10 nm (Full Wave at Half Maximum, FWHM). **Fig. 1c** exhibits the representative deflection (nm) vs. distance (nm) curves acquired from flagella (blue curve) and cell wall (green curve), by which the adhesion force of cell surface can be obtained. The measured results indicated, in **Fig. 1a**, that the adhesion force was 6.53 \pm 0.23 nN for flagella, and 4.78 \pm 0.28 nN for cell wall; for **Fig. 1b**, the adhesion force was measured at 5.69 \pm 0.10 nN for flagella, and 4.37 \pm 0.19 nN for cell wall. The statistics further revealed that the adhesion force of flagella is larger than that of the cell wall by 20~36%. It is also interesting to note that a similar phenomenon also appeared in our observation of another Gram-negative bacterium, *Escherichia coli* TOP10, whose flagella possess a larger adhesion force versus the cell wall by 17%~25%. The quantification of flagellum adhesion would facilitate a better understanding of the roles of flagella in bacterial motility related activities such as chemotaxis, bacterial infection and pathogenesis.

Interestingly, it should be noted that the characteristic “finger-print” structures at each of the two ends of a single KT2440 cell were easily seen (**Fig. 1d**), depicting the heterogeneous cell wall surface architectures; and such structural features commonly appeared on the polarized cell wall of KT2440 in the exponential growth phase. Furthermore, adhesion assessments revealed that the regions with “finger-print” features (two poles of bacterium) possessed a lower adhesion than the smooth “centre” region; for instance, the adhesion force for the centre region was measured at 7.13 \pm 0.05 nN, whereas that was 6.10 \pm 0.13 nN for the top pole, and 6.18 \pm 0.26 nN for the bottom pole (**Fig. 1d**). In addition, the adhesion forces of the corrugation ridge (red capital letters with yellow background) and corrugation trough (red capital letters with green background) (**Fig. 1e**) was measured at 5.58 \pm 0.10 nN and 5.74 \pm 0.07 nN, respectively. These forces were not statistically different, implying homogeneity in the adhesion property between the corrugation ridge and the corrugation trough of the cell wall polymer.

The heterogeneous surface architectures and adhesion force over the cell wall suggest that different biochemical constituents and/or biophysical behaviours; which, may correlate with the synthesis processes or rearrangement of bio-macromolecules in the cell wall. These structural features may be clues of bacterial activities during the progress of growth and division, such as the synthesis of peptidoglycan, lipopolysaccharide and other cell wall structures.

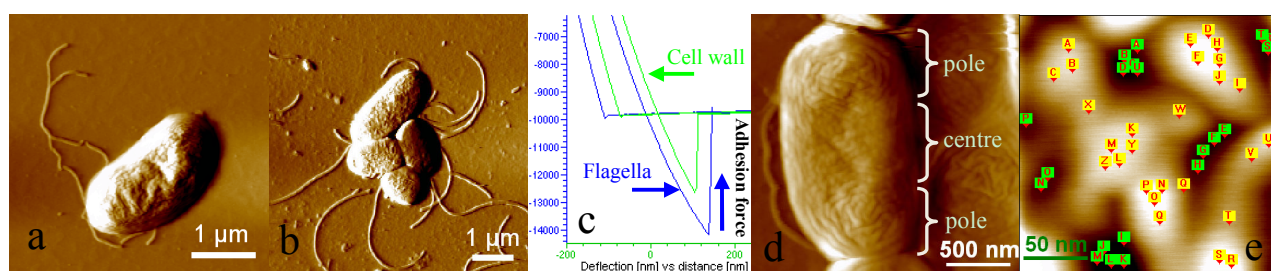


Fig. 1 Representative AFM images of *P. Putida* KT2440 (deflection mode), exhibiting obvious flagella around cells. (a) Single KT2440 cell; (b) cell colonies; (c) representative curves of deflection (nm) vs. distance (nm) measured from flagella (blue curve) and bacterial cell wall (green curve), by which bacterial adhesion force can be quantified; (d) a deflection mode image of KT2440, clearly showing the “finger-print” features at each end of cell (indicated by right brace and “pole”); (e) a representative nanostructural image of cell wall, displaying the two different locations (white and dark areas) from where adhesion force was measured.

3. AFM/Raman microspectroscopy for mammalian cancer cell characterization

3.1 Biological Background and Rationale

The mechanotransduction forces of mammalian cells are critical in the regulation of cell adhesion, migration, cell fate, and biochemical signals transduction [40-42]. The quantification of these mechanical properties (e.g. adhesion, elasticity and stiffness) for cancer cells is required for further interpreting respective biological processes (e.g. transformation, invasion, and metastasis). It is known that the mechanical properties, cell topography, membrane surface nanostructures, and cellular biochemical components vary among different cancer cell lines, and these differences are potentially connected to the development of new clinical diagnostic approaches [43-45]. Therefore, it is important to characterize the biophysical and biochemical differences among the cancer cell lines at the single cell and at sub-cellular level. In this subsection, metastatic human breast carcinoma cells MDA-MB-435 (435), non-metastatic MDA-MB-435/BRMS1 (435/BRMS1), and human lung adenocarcinoma epithelial cells (A549) were selected as model cell lines for evaluation of cell biomechanics of mammalian cells.

3.2 Sample preparation and AFM and Raman Imaging

435/BRMS1 cells were transfected with a lentiviral vector construct expressing full length BRMS1 cDNA under the control of a cytomegalovirus promoter. 435 and 435/BRMS1 cells were cultured in a 1:1 mixture of Dulbecco's-modified eagle's medium (DMEM) and Ham's F-12 medium supplemented with 5% fetal bovine serum (Hyclone, Logan, UT). Cells were cultured in 25-cm² Corning tissue culture dishes at 37 °C with 5% CO₂ in a humidified atmosphere. Human (*Homo sapiens*) lung carcinoma A549 cells (ATCC, USA) were cultured in F-12k medium containing 10% fetal bovine serum at 37 °C with 5% CO₂ in a humidified atmosphere. Cells were sub-cultured at 80-90% confluency and used for experiments. No antibiotics or antimycotics were used in cell cultures.

For AFM experiments, cells were seeded on poly-L-lysine coated Petri dishes at 5×10⁴ cells per mL. The same seeding density was used for Raman spectroscopy; only cells were seeded in quartz dishes (Quartz Scientific Inc., 313R020, USA) to minimize fluorescence background. Raman spectra for A549 cells were collected in an extended mode with 20 second laser exposure and were an average of four individual Raman spectra; 435 and 435/BRMS1 spectra were collected in an extended mode with 10 second laser exposure and were an average of ten individual Raman spectra. All wavenumber ranges for each spectra were truncated to 600 – 1800 cm⁻¹, Savitsky-Golay smoothed, and fluorescence corrected [39]. Raman spectral maps for A549 cells, 435, and 435/BRMS1 were imaged at a static wavenumber of ~1000 cm⁻¹ over a set range of ~805 - 1188 cm⁻¹, with 20 second exposure time at 100% laser power. All spectral maps were smoothed via bilinear interpolation.

In order to obtain nanomechanical properties of living cells, cultured cells were measured directly in culture medium without any pre-treatment to *in situ* measurements of biomechanical properties (e.g. adhesion behaviour, cellular elasticity). Also, the contact mode PicoPlus AFM was used to measure cells at room temperature. The spring constant of the cantilever was calibrated at 0.06 ~ 0.11 N/m (Veeco, USA). The approach/retract velocity applied throughout deflection (nm) vs. distance (nm) curve acquisition was 3.8 μm/s. The values for the adhesion force were also extracted using the SPIP software. The cellular spring constants (k_{cell}) were calculated using a previously proposed formula [46, 47]:

$$k_{cell} = -k_{tip} \cdot s / (1+s). \quad (1)$$

Where, s is the linear slope of the approaching branch, the ratio of *deflection (nm)* to *distance (nm)*; k_{cell} and k_{tip} represent the spring constants of cell and cantilever, respectively. All the data were reported as mean \pm SE (standard error of mean). The histograms were created using OriginPro 7.5 (OriginLab Corp., USA). The adhesion force or cellular spring constant maps were graphed with as 256 color maps created by Matlab version R2009a (MathWorks, Inc.).

3.3 Results and Quantification

To evaluate the nanomechanical differences among the three mammalian cell lines, the adhesion force (F) and cellular spring constant (k_{cell}) were analyzed *in situ* based on hundreds of force-distance curves for each cell type. Row 1, 2 and 3 in **Fig. 2** indicate a representative AFM image and the corresponding nanomechanical results of 435, 435/BRMS1 and A549 cells, respectively (column 1, AFM images; column 2, F maps; column 3, F histograms corresponding to column 2; column 4, k_{cell} maps; column 5, k_{cell} histograms corresponding to column 4). The low resolution images in **Fig. 2** (column 1) may arise from the soft cell membrane and the presence and movement of the membrane surface microvillus of living cells during tip scanning. Thus, AFM measurements were focused on the evaluation of nanomechanical properties of living cells. These indicated that the adhesion force and cell spring constant measured on one randomly selected 435 cell and A549 cell were significantly different ($p < 0.01$). Furthermore, to statistically assess the difference in nanomechanics among these three cell lines, twelve cells for each cell type were randomly selected for force measurement (26 datum points were collected on individual cells). The parametric statistical analysis (Student's t-test) showed that the mechanical properties of these cell lines are significantly different ($p < 0.01$). The measured adhesion forces were 0.43 ± 0.01 nN for 435 cell, 0.83 ± 0.01 nN for 435/BRMS1 cell, and 0.79 ± 0.01 nN for A549 cell. The measured cellular spring constants (k_{cell}) were 3.44 ± 0.06 mN/m for 435 cell, 4.33 ± 0.07 mN/m for 435/BRMS1, and 4.83 ± 0.11 mN/m for A549 cell. Such data clearly exhibited that BRMS1 expression elevated cellular nanomechanics (e.g. cell elasticity, adhesion force) [17], which largely arises from reorganization of the cytoskeleton, variation of cytoarchitectures (cell topography and nanostructures), and changes of extracellular matrix of 435 cells [48]. And the statistical analysis presented here also showed that lung cancer cell A549 possesses a different membrane surface adhesion force and cell elasticity compared to breast cancer cell lines 435 and 435/BRMS1; which, could be ascribed to the different cell lines possessing different in biochemical components and biophysical properties. This work and others [43-45, 49-52] illustrate the potential of AFM application in identifying cancer cells, especially, for metastatic and non-metastatic cancer cells.

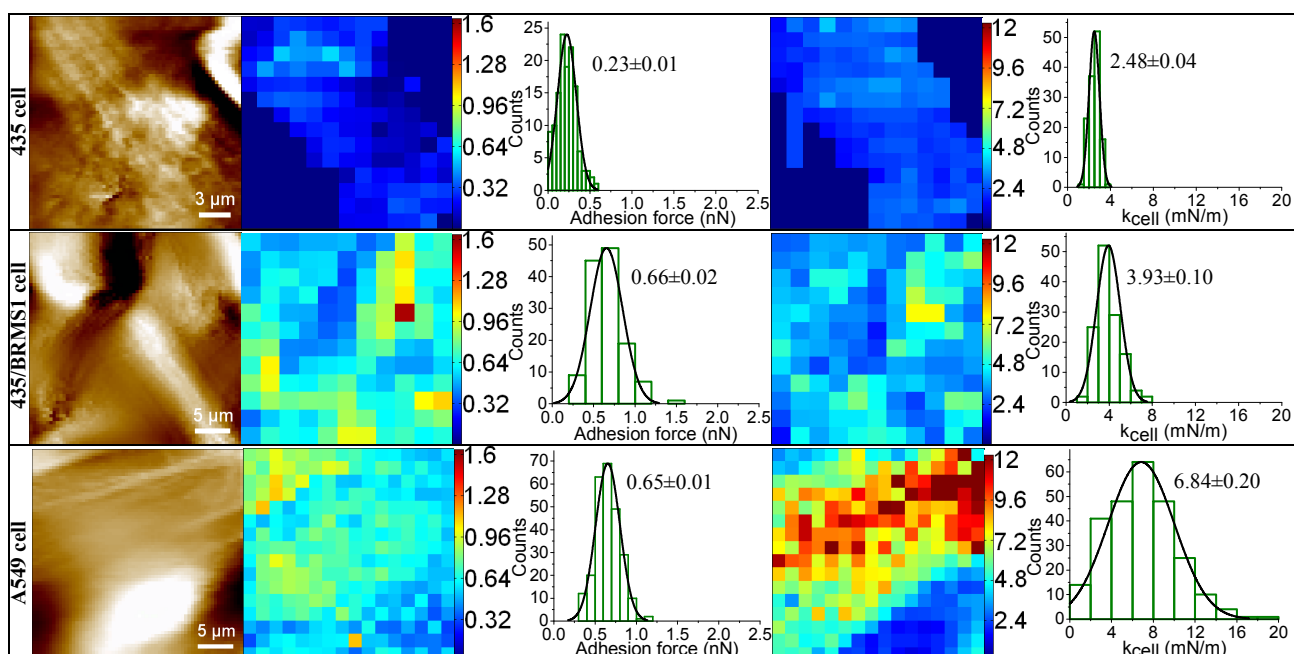


Fig. 2 Biomechanical evaluation of living breast carcinoma cell lines 435 (row 1) and 435/BRMS1 cells (row 2), and lung cancer cell line A549 (row 3). Column 1 shows representative topography images acquired in culture medium. The color maps of adhesion force (F) and spring constant (k_{cell}) measured from single 435 cell, 435/BRMS1 cell and A549 cell (column 1) are shown as column 2 and column 4, respectively, and their respective distribution histogram (mean \pm SE is marked) is displayed as column 3 and column 5, respectively. The color bars arranged at the right of color maps illustrate the value scale of color-coded maps of adhesion force (nN) and k_{cell} (mN/m).

Stacked Raman spectra of *P. putida* KT2440, A549, 435, and 435/BRMS1 are illustrated in **Fig. 3**. Each Raman spectral fingerprint illustrates the complex nature of the biological organism based upon the numerous spectral peaks or

Raman bands, which are associated with the complex biochemical make-up of the bacterial organism or mammalian cell line. It is interesting to note that there is great overlap in many of these characteristic Raman bands. For example all spectra in **Fig. 3(a-d)** share specific bands at $\sim 624, 644, 670, 787, 813, 940, 1006, 1130, 1158, 1265, 1345, 1452, 1580,$ and 1663 cm^{-1} , respectively. These bands are tentatively assigned as follows; 624 (unidentified), 644 (C-C twisting mode of tyrosine), 670 (C-S stretching mode of cytosine or T/G in DNA/RNA), 787 (relative quantity of present nucleic acid), 813 (characteristic RNA band), 940 (C-C stretch backbone), 1006 (carotenoids/ring breathing phenylalanine), 1130 (C-C skeletal stretch), 1158 (C-C/C-N stretching of proteins), 1265 (Amide III), 1345 (δCH residual vibrations), 1452 (CH_2CH_3 deformation/protein bands), 1580 (C-C stretching), and 1663 cm^{-1} (Amide I) [53]. **Fig. 3a** includes distinct Raman bands at ~ 746 (T ring breathing mode of DNA/RNA bases), 850 (amino acid, valine, or polysaccharide single bond stretching vibration), 891 (saccharide band), 964 (unassigned protein band), and 1084 cm^{-1} (phosphodiester groups in nucleic acids) respectively [53]. **Fig. 3b** contains a few distinct bands at ~ 730 (adenine), 1050 (unassigned), 1318 (G ring breathing modes of DNA/RNA or C-H deformation in protein), and 1424 cm^{-1} (deoxyribose, B,Z-marker) [53] also **Fig. 3c, d** contains distinct bands at ~ 720 (DNA), 760 (tryptophan ring deformation or breathing mode in protein), 1303 (CH_3, CH_2 twisting collagen), 1555 (Amide II), and 1608 cm^{-1} (cytosine) respectively [53]. These Raman spectroscopy results, specifically those for A549, 435 and 435/BRMS1, implying the different biochemical structures among these model cell lines. The findings support the AFM results that also revealed different biochemical components and biophysical properties of these cell lines.

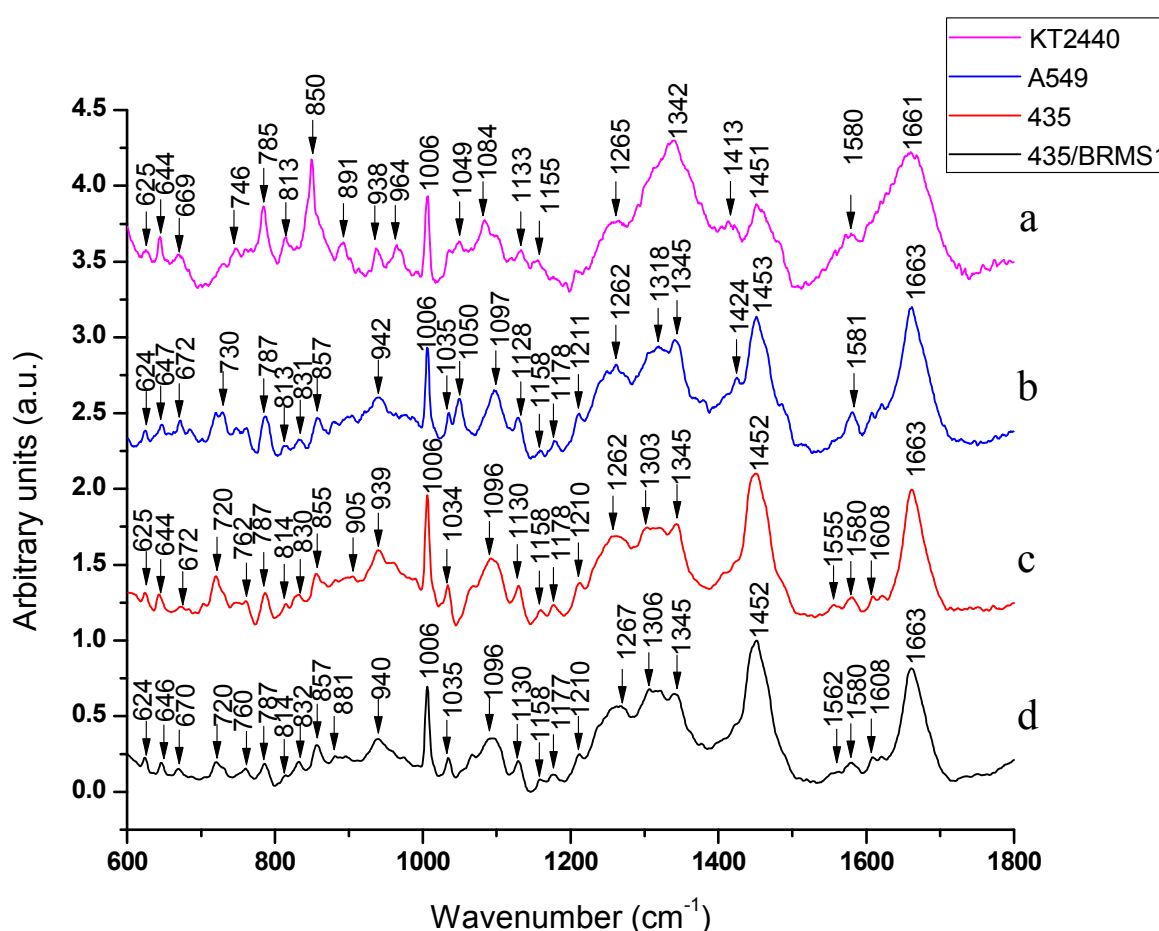


Fig. 3 Representative bulk Raman spectrum of *Pseudomonas putida* KT2440 imaged on agar after 24 hour culture period (a). Raman spectrum of A549 cells imaged on quartz (b), 435 cells imaged on quartz (c), and 435/BRMS1 cells imaged on quartz (d). All mammalian cells were imaged when within 24-48 hours of subculture.

Raman spectral mapping (**Fig. 4**) was performed on each biological sample: KT2440, A549, 435 and 435/BRMS1. Each map was centered at $\sim 1006 \text{ cm}^{-1}$ for protein and Raman spectra at each point within the map were collected at 45 second exposure for KT2440 and 20 second exposure time for A549, 435 and 435/BRMS1. At first glance, the overall component distribution for KT2440, A549, 435 and 435/BRMS1 (**Fig. 4b, d, f, h**) appeared very similar, with the exception of the sample morphology. Closer observation reveals that the mammalian cell lines (**Fig. 4d, f, h**), as compared with KT2440 (**Fig. 4b**), have an overall similar distribution of protein with stronger intensities at the cell

nucleus and decreasing intensities in the cytoplasm and at the peripheral membrane. Conversely, the Raman spectral map of KT2440 is of a bacterial mass or colony and yet similarly demonstrates that the greater concentration of proteins lies at the interior mass of this bacterial colony and diminishes outside the core of the colony.

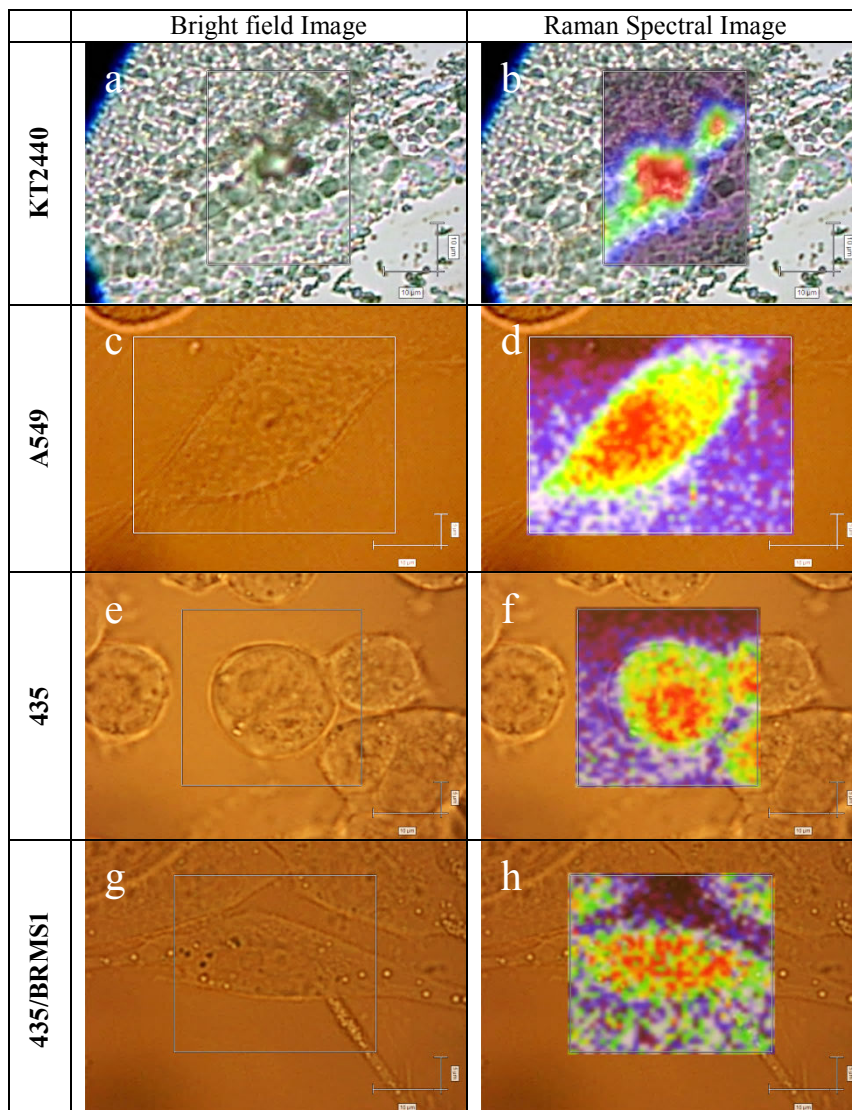


Fig. 4 Raman spectral image of bulk biochemical information for *P. putida* KT2440, A549, 435, and 435/BRMS1 cells; bright field view (a, c, e, and g) and respective overlay Raman images (b, d, f, and h). Raman spectral image for KT2440 was imaged at a static wavenumber of 1006 cm^{-1} over a set range of $\sim 816 - 1186\text{ cm}^{-1}$, with 45 second exposure time at 100% laser power, scale bars are $10\text{ cm} \times 5\text{ cm}$. Raman spectral maps for A549, 435, and 435/BRMS1 were imaged at a static wavenumber of $\sim 1000\text{ cm}^{-1}$ over a set range of $\sim 805 - 1188\text{ cm}^{-1}$, with 20 second exposure time at 100% laser power, scale bars are $10\text{ cm} \times 10\text{ cm}$.

4. Summary

The AFM investigations revealed the characteristic “finger-print” structures at the two ends of KT2440 cells, and quantified that the adhesion force of flagella is larger than that of cell wall by 20~36%. Raman was able to reveal biochemical structural components of bacterial EPS of KT2440 by native Raman bands within a bulk Raman spectra. For the mammalian cancer cell lines, AFM and Raman were both useful to assess and compare the difference in nanomechanics and biochemical compositions among the three cancer cell lines. The AFM measurements showed that A549 cells possessed a larger adhesion force and cell elasticity than 435 cells, and that BRMS1-expression elevated the adhesion force and cell elasticity in 435/BRMS1 cells. Raman spectra illustrated an overall similarity among A549, 435 and 435/BRMS1. In 435 and 435/BRMS1 cells there is a slightly weaker Raman band intensity observed in 435/BRMS1 cells. That could imply that BRMS1 suppressor gene expression may not significantly change, or these changes are not detectable under current experimental conditions, the cellular biochemical compositions, but may slightly alter the intensities (amount or distribution) of these biochemical components on the cell surface [17].

AFM and Raman microspectroscopy provide new access to cell mechanics, cytoarchitectures and biochemical components of cancer cells [18, 43-45, 50, 54, 55] at the single cell and sub-cellular levels and could be utilized as a force and optical “biomechanical marker” technique for the development of a new tool for early diagnosis of cancer.

Acknowledgements This work is partially supported by Utah Water Research Laboratory and USU Huntsman Environmental Research Center (A.Z.). The Raman microscope was acquired under a DoD Grant (#W911NF-06-01-0139) (A.Z.). G.M. thanks the support of USU Graduate Fellowship. We are grateful to Dr. Daryll DeWald’s laboratory providing MDA-MB-435 and MDA-MB-435/BRMS1 cell lines.

References

- [1] Binnig G, Quate CF, Gerber C. Atomic force microscope. *Physical review letters*. 1986;56:930-3.
- [2] Butt HJ, Cappella B, Kappl M. Force measurements with the atomic force microscope: Technique, interpretation and applications. *Surface Science Reports*. 2005;59:1-152.
- [3] Parot P, Dufrene YF, Hinterdorfer P, et al. Past, present and future of atomic force microscopy in life sciences and medicine. *J Mol Recognit*. 2007;20:418-31.
- [4] Li L, Chen S, Oh S, Jiang S. In situ single-molecule detection of antibody-antigen binding by tapping-mode atomic force microscopy. *Anal Chem*. 2002;74:6017-22.
- [5] Lyubchenko YL, Shlyakhtenko LS. Visualization of supercoiled DNA with atomic force microscopy in situ. *Proc Natl Acad Sci U S A*. 1997;94:496-501.
- [6] Hirano Y, Takahashi H, Kumeta M, et al. Nuclear architecture and chromatin dynamics revealed by atomic force microscopy in combination with biochemistry and cell biology. *Pflugers Arch*. 2008;456:139-53.
- [7] Dufrene YF. Atomic force microscopy, a powerful tool in microbiology. *J Bacteriol*. 2002;184:5205-13.
- [8] Horber JK, Miles MJ. Scanning probe evolution in biology. *Science (New York, NY)*. 2003;302:1002-5.
- [9] Rösch P, Harz M, Schmitt M, et al. Chemotaxonomic Identification of Single Bacteria by Micro-Raman Spectroscopy: Application to Clean-Room-Relevant Biological Contaminations. *Appl Environ Microbiol*. 2005;71:1626-37.
- [10] McEwen GD, Wu Y, Zhou A. Probing nanostructures of bacterial extracellular polymeric substances versus culture time by Raman microspectroscopy and atomic force microscopy. *Biopolymers*. 2009;93:171-7.
- [11] Ling J, Weitman SD, Miller MA, Moore RV, Bovik AC. Direct Raman Imaging Techniques for Study of the Subcellular Distribution of a Drug. *Appl Opt*. 2002;41:6006-17.
- [12] Petrov GI, Arora R, Yakovlev VV, Wang X, Sokolov AV, Scully MO. Comparison of coherent and spontaneous Raman microspectroscopies for noninvasive detection of single bacterial endospores. *Proceedings of the National Academy of Sciences*. 2007;104:7776-9.
- [13] Rösch P, Schmitt M, Kiefer W, Popp J. The identification of microorganisms by micro-Raman spectroscopy. *Journal of Molecular Structure*. 2003;661-662:363-9.
- [14] De Gelder J, De Gussem K, Vandenabeele P, Vancanneyt M, De Vos P, Moens L. Methods for extracting biochemical information from bacterial Raman spectra: Focus on a group of structurally similar biomolecules--Fatty acids. *Analytica Chimica Acta*. 2007;603:167-75.
- [15] Baena JR, Lendl B. Raman spectroscopy in chemical bioanalysis. *Current Opinion in Chemical Biology*. 2004;8:534-9.
- [16] Carey PR. Raman Spectroscopy, the Sleeping Giant in Structural Biology, Awakes. *J Biol Chem*. 1999;274:26625-8.
- [17] Wu Y, McEwen GD, Harihar S, Baker SM, DeWald DB, Zhou A. BRMS1 expression alters the ultrastructural, biomechanical and biochemical properties of MDA-MB-435 human breast carcinoma cells: an AFM and Raman microspectroscopy study. *Cancer Lett*. 2010;293:82-91.
- [18] Yu C, Gestl E, Eckert K, Allara D, Irudayaraj J. Characterization of human breast epithelial cells by confocal Raman microspectroscopy. *Cancer Detection and Prevention*. 2006;30:515-22.
- [19] Krishna CM, Sockalingum GD, Kegelaer G, Rubin S, Kartha VB, Manfait M. Micro-Raman spectroscopy of mixed cancer cell populations. *Vibrational Spectroscopy*. 2005;38:95-100.
- [20] Carey P. Raman spectroscopy for the analysis of biomolecules. *TrAC Trends in Analytical Chemistry*. 1983;2:275-7.
- [21] Pappas D, Smith BW, Winefordner JD. Raman spectroscopy in bioanalysis. *Talanta*. 2000;51:131-44.
- [22] Hildebrandt P, Lecomte S, John CL. Biochemical Applications of Raman Spectroscopy. *Encyclopedia of Spectroscopy and Spectrometry*. Oxford: Elsevier 1999:88-97.
- [23] Fabian H, Anzenbacher P. New developments in Raman spectroscopy of biological systems. *Vibrational Spectroscopy*. 1993;4:125-48.
- [24] Lyng FM, Faoláin EÓ, Conroy J, et al. Vibrational spectroscopy for cervical cancer pathology, from biochemical analysis to diagnostic tool. *Experimental and Molecular Pathology*. 2007;82:121-9.
- [25] Tripathi A, Jabbour RE, Guicheteau JA, et al. Bioaerosol Analysis with Raman Chemical Imaging Microspectroscopy. *Analytical Chemistry*. 2009;81:6981-90.
- [26] Guicheteau J, Argue L, Emge D, Hyre A, Jacobson M, Christesen S. Bacillus Spore Classification via Surface-Enhanced Raman Spectroscopy and Principal Component Analysis. *Appl Spectrosc*. 2008;62:267-72.
- [27] Brozek-Pluska B, Placek I, Kurczewski K, Morawiec Z, Tazbir M, Abramczyk H. Breast cancer diagnostics by Raman spectroscopy. *Journal of Molecular Liquids*. 2008;141:145-8.
- [28] Chowdary MVP, Kumar KK, Stanley M, Lakshmi R, Krishna CM, Jacob K. Biochemical correlation of Raman spectra of normal, benign and malignant breast tissues: A spectral deconvolution study. *Biopolymers*. 2009;91:539-46.
- [29] Kanter EM, Majumder S, Kanter GJ, Woeste EM, Mahadevan-Jansen A. Effect of hormonal variation on Raman spectra for cervical disease detection. *American Journal of Obstetrics and Gynecology*. 2009;200:512.e1-e5.

- [30] Kanter EM, Majumder S, Vargis E, et al. Multiclass discrimination of cervical precancers using Raman spectroscopy. *Journal of Raman Spectroscopy*. 2009;40:205-11.
- [31] Beljebbar A, Bouché O, Diébold MD, et al. Identification of Raman spectroscopic markers for the characterization of normal and adenocarcinomatous colonic tissues. *Critical Reviews in Oncology/Hematology*. 2009;72:255-64.
- [32] Baulig A, Sourdeval M, Meyer M, Marano F, Baeza-Squiban A. Biological effects of atmospheric particles on human bronchial epithelial cells. Comparison with diesel exhaust particles. *Toxicology in Vitro*. 2003;17:567-73.
- [33] Pyrgiotakis G, Bhowmick TK, Finton K, et al. Cell (A549)-Particle (<I>Jasada Bhasma</I>) interactions using Raman spectroscopy. *Biopolymers*. 2008;89:555-64.
- [34] Tortora GJ, Funke BR, Case CL. Microbiology An Introduction. 6 ed: Addison Wesley Longman, Inc., Menlo Park-California 1998.
- [35] Burks GA, Velegol SB, Paramonova E, Lindenmuth BE, Feick JD, Logan BE. Macroscopic and Nanoscale Measurements of the Adhesion of Bacteria with Varying Outer Layer Surface Composition. *Langmuir*. 2003;19:2366-71.
- [36] Bagdasarian M, Lurz R, Rückert B, et al. Specific-purpose plasmid cloning vectors. II. Broad host range, high copy number, RSF1010-derived vectors, and a host-vector system for gene cloning in *Pseudomonas*. *Gene*. 1981;16:237-47.
- [37] Karen EN. The complete genome sequence of *Pseudomonas putida* KT2440 is finally available. *Environmental Microbiology*. 2002;4:777-8.
- [38] Register F. Certified host-vector systems. Washington, DC 1982.
- [39] Zhao J, Lui H, McLean DI, Zeng H. Automated Autofluorescence Background Subtraction Algorithm for Biomedical Raman Spectroscopy. *Appl Spectrosc*. 2007;61:1225-32.
- [40] Janmey PA, McCulloch CA. Cell mechanics: Integrating cell responses to mechanical stimuli. *Annu Rev Biomed Eng*. 2007;9:1-34.
- [41] Kim DH, Wong PK, Park J, Levchenko A, Sun Y. Microengineered platforms for cell mechanobiology. *Annu Rev Biomed Eng*. 2009;11:203-33.
- [42] Janmey PA, McCulloch CA. Cell mechanics: Integrating cell responses to mechanical stimuli. *Annual Review of Biomedical Engineering*. 2007;9:1-34.
- [43] Cross SE, Jin YS, Rao J, Gimzewski JK. Nanomechanical analysis of cells from cancer patients. *Nature Nanotechnology*. 2007;2:780-3.
- [44] Suresh S. Nanomedicine - Elastic clues in cancer detection. *Nature Nanotechnology*. 2007;2:748-9.
- [45] Suresh S. Biomechanics and biophysics of cancer cells. *Acta Biomaterialia*. 2007;3:413-38.
- [46] Velegol SB, Logan BE. Contributions of bacterial surface polymers, electrostatics, and cell elasticity to the shape of AFM force curves. *Langmuir*. 2002;18:5256-62.
- [47] Arnoldi M, Fritz M, Bauerlein E, Radmacher M, Sackmann E, Boulbitch A. Bacterial turgor pressure can be measured by atomic force microscopy. *Physical Review E*. 2000;62:1034-44.
- [48] Champine PJ, Michaelson J, Weimer BC, Welch DR, DeWald DB. Microarray analysis reveals potential mechanisms of BRMS1-mediated metastasis suppression. *Clin Exp Metastasis*. 2007;24:551-65.
- [49] Cross SE, Jin YS, Tondre J, Wong R, Rao J, Gimzewski JK. AFM-based analysis of human metastatic cancer cells. *Nanotechnology*. 2008;19:384003-11.
- [50] Li QS, Lee GY, Ong CN, Lim CT. AFM indentation study of breast cancer cells. *Biochem Biophys Res Commun*. 2008;374:609-13.
- [51] Lekka M, Laidler P, Gil D, Lekki J, Stachura Z, Hryniewicz AZ. Elasticity of normal and cancerous human bladder cells studied by scanning force microscopy. *European Biophysics Journal with Biophysics Letters*. 1999;28:312-6.
- [52] Lam WA, Rosenbluth MJ, Fletcher DA. Chemotherapy exposure increases leukemia cell stiffness. *Blood*. 2007;109:3505-8.
- [53] Movasaghi Z, Rehman S, Rehman IU. Raman Spectroscopy of Biological Tissues. *Applied Spectroscopy Reviews*. 2007;42:493 - 541.
- [54] Kendall C, Isabelle M, Bazant-Hegemark F, et al. Vibrational spectroscopy: a clinical tool for cancer diagnostics. *Analyst*. 2009;134:1029-45.
- [55] Cross SE, Jin YS, Tondre J, Wong R, Rao J, Gimzewski JK. AFM-based analysis of human metastatic cancer cells. *Nanotechnology*. 2008;19:384003 (8 pp).